# Simulating radial diffusion of energetic (MeV) electrons through a model of fluctuating electric and magnetic fields

T. Sarris, Xiaojian Li, M. Temerin

Ann. Geophys., 24, 2583–2598, 2006
www.ann-geophys.net/24/2583/2006/


Annales Geophysicae

# Simulating radial diffusion of energetic (MeV) electrons through a model of fluctuating electric and magnetic fields

**T. Sarris**[1,2], **X. Li**[1], **and M. Temerin**[3]

[1]Lab. for Atmospheric and Space Physics, Univ. of Colorado, Boulder, CO, USA
[2]Demokritus University of Thrace, Xanthi, Greece
[3]Space Sciences Lab, University of California, Berkeley, CA, USA

Received: 29 March 2006 – Revised: 4 July 2006 – Accepted: 19 July 2006 – Published: 20 October 2006

**Abstract.** In the present work, a test particle simulation is performed in a model of analytic Ultra Low Frequency, ULF, perturbations in the electric and magnetic fields of the Earth's magnetosphere. The goal of this work is to examine if the radial transport of energetic particles in quiet-time ULF magnetospheric perturbations of various azimuthal mode numbers can be described as a diffusive process and be approximated by theoretically derived radial diffusion coefficients. In the model realistic compressional electromagnetic field perturbations are constructed by a superposition of a large number of propagating electric and consistent magnetic pulses. The diffusion rates of the electrons under the effect of the fluctuating fields are calculated numerically through the test-particle simulation as a function of the radial coordinate $L$ in a dipolar magnetosphere; these calculations are then compared to the symmetric, electromagnetic radial diffusion coefficients for compressional, poloidal perturbations in the Earth's magnetosphere. In the model the amplitude of the perturbation fields can be adjusted to represent realistic states of magnetospheric activity. Similarly, the azimuthal modulation of the fields can be adjusted to represent different azimuthal modes of fluctuations and the contribution to radial diffusion from each mode can be quantified. Two simulations of quiet-time magnetospheric variability are performed: in the first simulation, diffusion due to poloidal perturbations of mode number $m$=1 is calculated; in the second, the diffusion rates from multiple-mode ($m$=0 to $m$=8) perturbations are calculated. The numerical calculations of the diffusion coefficients derived from the particle orbits are found to agree with the corresponding theoretical estimates of the diffusion coefficient within a factor of two.

*Correspondence to:* T. Sarris
(tsarris@ee.duth.gr)

**Keywords.** Magnetospheric physics (Energetic particles, trapped) – Space plasma physics (Charged paricle motion and acceleration; Numerical simulation studies)

## 1 Introduction

Determining the source and acceleration mechanism of energetic (MeV) particles is one of the main current subjects of research in radiation belt physics. It has been observed that often during periods of magnetic activity, combined with high solar wind velocity, electron acceleration occurs, evidenced by MeV electron flux increases by a few orders of magnitude on time scales from hours to days (e.g. Paulikas and Blake, 1979; Baker et al., 1986). Many different acceleration and loss processes might occur during such times, acting on particles either adiabatically or non-adiabatically, depending on the time scale of each process. A review of the various transport and acceleration mechanisms that have been proposed to explain the orders-of-magnitude increase of particle fluxes is given in Li and Temerin (2001) and Fridel et al. (2002); a differentiation between the various mechanisms in terms of the changes they inflict on phase-space density is presented in Green and Kivelson (2004).

Radial diffusion was one of the mechanisms proposed early in radiation belt research to explain these large electron flux increases. The underlying principle in radial diffusion theory is that irregular fluctuations of the electromagnetic fields in the magnetosphere on the time scale of the bounce-averaged drift period of energetic particles violate the third adiabatic invariant of the particles and can cause a random radial motion in their orbits. An electron that moves to a lower $L$-shell and a stronger magnetic field gains energy, whereas an electron that moves outward to larger $L$-shells loses en-

Published by Copernicus GmbH on behalf of the European Geosciences Union.

ergy. Such stochastic diffusion in the electrons' $L$-shell will result in a net increase or decrease on particle flux at a given location and energy, depending on the initial distribution of particles, and also on the existence of particle sources and losses in the magnetosphere. As Kivelson and Russel (1995) note, radial diffusion always has the effect of reducing the radial gradients of the distribution function at fixed first and second adiabatic invariants, $\mu$ and $J$. It remains to be seen if radial diffusion caused by ULF waves is capable of transporting enough plasma sheet particles into the inner magnetosphere to explain the orders-of-magnitude increases in the fluxes that are often observed in the inner magnetosphere. It also remains open to quantify the contribution from various modes of ULF perturbations and to associate the contribution with the perturbations' excitation mechanism.

Theoretical estimates of the diffusion rates of electrons, due to stochastic electric and magnetic perturbations, have been performed since the early years of radiation belt studies (Falthammar, 1965; and later on, Schultz and Lanzerotti, 1974; Brizard and Chan, 2001). In these studies, the derived expressions for the diffusion rates are related to the spectral characteristics of broad-band magnetospheric random variations. The diffusion rate of energetic electrons is described by the diffusion coefficient, $D_{LL}$. The expression for the diffusion coefficient of electrons in fluctuating fields was introduced by Falthammar (1965), who also made a distinction between electrostatic ($D_{LL}^{E}$) and electromagnetic ($D_{LL}^{M}$) contributions to the total diffusion coefficient $D_{LL}$, and derived expressions for $D_{LL}^{E}$ and $D_{LL}^{M}$ as a function of $L$. Electrostatic diffusion is caused by perturbations in the convection electric fields, whereas electromagnetic diffusion is caused by perturbations in the Earth's magnetic field and by the induced perturbating electric fields. The expressions for $D_{LL}^{E}$ and $D_{LL}^{M}$ were also found to be dependent on the spectral power density of the fluctuating fields, and in particular, on the power spectral density at the particles' drift frequency, since only fluctuations at frequencies close to the electrons' drift frequencies can produce enhanced diffusion, through the drift-resonant interaction between ULF waves and the electrons. These derivations were non-relativistic and included contributions only from $m$=1 mode, where $m$ is the azimuthal wave number (for a definition of $m$, see below, Sect. 4.1.3). Recently, using a treatment similar to Falthammar (1965), Fei et al. (2006) derived theoretical calculations for the electric and magnetic diffusion coefficients of relativistic electrons in a symmetric and an asymmetric magnetic field that included contributions from different modes.

Radial diffusion mechanisms have been used in various efforts to model radiation belt dynamics during different types of geomagnetic conditions. Modeling of outer zone electrons during a storm by Brautigam and Albert (2000) has indicated that additional heating by in-situ acceleration mechanisms was required to reproduce the observed electron fluxes of higher $\mu$, while the flux enhancement of lower $\mu$ was adequately described by radial diffusion. A review of modeling efforts by Albert et al. (2001) concluded that radial diffusion provides an underlying and significant minimum level of transport that must be considered, and suggested that existing radial diffusion formalism could be expanded to incorporate other acceleration mechanisms. Radial diffusion calculations have also been performed using semi-empirical radial diffusion coefficients that successfully model and predict MeV electron fluxes at geosynchronous orbit, based on solar wind measurements (Li et al., 2001; Li, 2004). Numerical tests of radial diffusion in modeled field fluctuations have been performed in various studies: Elkington et al. (1999, 2003) investigated the interaction of particles in global, low-$m$ toroidal mode waves and found increased diffusion due to drift-resonance interactions; they associated the efficiency of radial diffusion processes to various characteristics of the magnetospheric variations, such as power spectral density, the presence of non-axisymmetric magnetic field, superimposed toroidal oscillations, and strong convection electric fields. Perry et al. (2005) investigated the effects of magnetic and electric fields associated with poloidal mode ULF waves in a three-dimensional guiding center test particle code from which the $L$, energy, and pitch angle dependence of the diffusion rates were analyzed. Results from a dipole magnetic field model were compared to a compressed dipole model in the equatorial plane, and diffusion rates were shown to depend more strongly on $L$ than assumed in previous studies, particularly in times of intense ULF activity. Ukhorskiy et al. (2005) traced particles in narrow-band ULF waves with amplitudes similar to those often observed at CRRES, and found the diffusion rates due to toroidal waves to be very low; they also found that poloidal mode waves provide a much more efficient form of radial diffusion and therefore can play an important role in the dynamics of the outer radiation belt. Fei et al. (2006) used power spectral densities calculated from the MHD waves, produced by a global MHD simulation of a magnetic storm; test particles were traced in the global MHD fields, and their study showed that the radial diffusion coefficients describe the electron transport quite well, with the asymmetric terms making significant contributions at larger $L$-shells.

Irregular fluctuations of the electromagnetic fields in a dipolar magnetosphere will generally cause two distinct modes of oscillation in cold plasma, referred to as the toroidal and the poloidal modes (Alfvén and Falthammar, 1963; Dungey, 1963). Toroidal oscillations are field-line resonances, caused by standing Alfvén waves on geomagnetic field lines. Solar wind driven Kelvin-Helmholtz waves traveling on the magnetopause can excite such oscillations on field lines deep within the magnetosphere (Southwood, 1974; Chen and Hasegawa, 1974). They are characterized by azimuthal magnetic field perturbations and radial electric field perturbations. The polarization of these oscillations is elliptic and shows a reversal of its direction of rotation in the noon to post-noon region, and also at the midnight to post-

midnight region (Walker et al., 2005, pp. 233–244, and references therein). These oscillations can be described as coherent global oscillations of a magnetospheric $L$-shell with perturbations in the azimuthal directions. Poloidal oscillations, on the other hand, take place in the magnetic meridian (e.g. Anderson et al., 1990), i.e. the poloidal direction; they are characterized by $z$-direction (perpendicular to the equatorial plane) or radial direction magnetic field perturbations and azimuthal electric field perturbations. Poloidal oscillations are also referred to as compressional and fast mode waves; they can be caused by either external perturbations at or beyond the magnetopause, or by internal ion anisotropies within the magnetosphere. In one description, poloidal oscillations can be excited by solar wind impulses incident upon the magnetospheric cavity; these waves can reflect and become standing between an outer boundary (possibly the magnetopause) and a turning point within the magnetosphere (e.g. Mann and Wright, 1995). Poloidal oscillations could also be a consequence of mirror instability (e.g. Walker et al., 2005, pp. 233–244). It has been demonstrated by theoretical calculations and computer simulations that poloidal waves can be mode-converted to toroidal waves which are resonantly excited on closed magnetic field lines where the frequency of the poloidal waves matches the local Alfvén frequency (Kivelson and Southwood, 1985; Wright and Rickard, 1995). In the process they transfer their perturbation energy and are thus dampened.

In this paper we present a model of random field fluctuations that aims in reproducing poloidal, compressional perturbations of various modes. In this model, random field fluctuations are created by a superposition of earthward propagating Gaussian electric and consistent magnetic pulses that are reflected 100% at an inner limit. They are superimposed on a symmetric background magnetic field. The superposition of the randomly initialized pulses produces a broadband fluctuation in the magnetic and electric fields that mimics well the observed spectral characteristics at geosynchronous orbit. The magnetic field pulses have a northward component and the consistent electric field has an azimuthal component; thus, based on the results from previous research and also based on the observational characteristics that are described in the next section, we assume in the following that the field perturbations represent poloidal, compressional, fast-mode (also called storm-time) ULF pulsations.

Energetic electrons are traced under the effect of the modeled fluctuating fields, and the diffusion rates of the electrons are calculated numerically. In this study we focus on energetic electrons in the energy range from hundreds of keV to a few MeV. We are particularly interested in electrons of these energies since they are often of significant flux to cause spacecraft malfunctions and pose threats to astronauts in the inner magnetosphere (e.g. Gussenhoven et al., 1991; Baker et al., 1998a, 1994). The frequency range of ULF perturbations that is close to the drift frequency of these electrons is 1.5 to 10 mHz, and has been termed the Pc-5 range (see

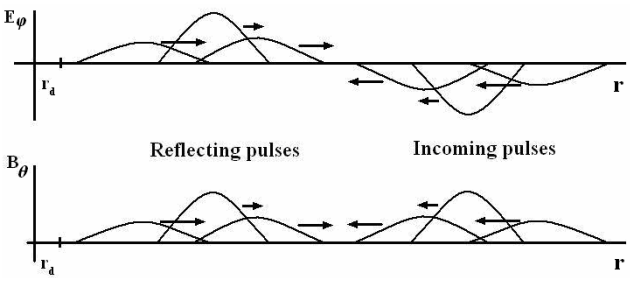


**Fig. 1.** The field fluctuations are produced in the model by the superposition of a large number of electromagnetic Gaussian pulses that propagate earthward and are reflected 100% at an inner boundary $r_d$.

classification by Jacobs et al., 1964).

Two different azimuthal localizations of poloidal compressional pulsations are simulated: pulsations that extend across the whole dayside magnetosphere and have a null at midnight, and pulsations extending across a fraction of the dayside region. The two simulations of different azimuthal extents are compared to the azimuthal modes of compressional fluctuations; the first case simulates fluctuations with contributions from the primary, global-oscillation mode ($m$=0) and first mode ($m$=1), whereas the second case simulates a localized fluctuation with contribution from modes, with mode numbers $m$=0 to $m$=8. In the simulated fluctuations we trace relativistic electrons of single-$\mu$ values. Through their radial displacement in time, we calculate the diffusion rates of the electrons for the two cases. The diffusion rates obtained through the simulation are compared to existing theoretical calculations, which associate the diffusion rate of the electrons with the Power Spectral Density, PSD, of the fluctuations.

## 2 Observations

The model presented in this work simulates compressional Pc-5 fluctuations in the magnetosphere. Some of the reported characteristics of compressional fluctuations, as derived from observations and modeling, are the following:

1. Compressional Pc-5 pulsations, as well as toroidal and poloidal mode field line resonances appear to account for most of the observed pulsations in the outer magnetosphere (Anderson et al., 1990). In their study, Anderson et al. recorded pulsations as compressional when the dominant spectral feature appeared in the radial and northward components.

2. Most of the ULF pulsations are observed in the dayside (Arthur et al., 1977; Takahashi and McPherron, 1982; Anderson et al., 1990). They are thought to originate outside the magnetosphere (Yumoto, 1988). Possible

sources are the solar wind (Barnes, 1983), the foreshock (Greenstadt et al., 1980), the bow shock (Greenstadt et al., 1979; Takahashi et al., 1981) and the magnetopause (Kepko et al., 2002).

3. Storm-time compressional pulsations are localized in latitude, occurring within 15° of the magnetic equator. Storm-time Pc-5 type waves display a systematic variation in latitude distribution with $L$, being more localized near the equator for low $L$ than for high $L$ (Anderson et al., 1990).

4. Compressional pulsations have been observed between 8 and 12 $R_E$ near dusk with HEOS 1 (Hedgecock, 1976), suggesting that a significant number of these waves occur at distances greater than 6.6 $R_E$.

5. The power of compressional pulsations in the Pc-5 frequency range is enhanced characteristically during the main phase of magnetic storms (Baker et al., 1998b; O'Brien et al., 2001), establishing the link between the solar wind and magnetospheric Pc-5 fluctuations.

6. The propagation of a disturbance in the magnetosphere has been modeled several decades ago (e.g. Francis et al., 1959; Nishida, 1964; Burlaga & Ogilvie, 1969). In some descriptions, solar wind impulses incident upon the magnetospheric cavity can excite inward traveling compressional impulses which propagate with the speed of a fast mode, magnetosonic wave.

7. Compressional waves propagating within the magnetospheric cavity can reflect and become standing between the magnetopause and a turning point within the magnetosphere (Mann and Wright, 1995), which could be the plasmapause.

8. As compressional impulses propagate into the magnetosphere across magnetic shells, they continuously produce transverse waves via mode conversion due to the inhomogeneity of the propagation media (ring-current and plasmaspheric plasma) and also because of the curved geometry (Hasegawa et al., 1983; Mann and Wright, 1995). Thus, polarization and amplitude, as well as arrival times based on any local measurements are expected to strongly depend on wave coupling and dipolar geometry in the magnetosphere (Lee & Lysak, 1999).

## 3 Model Description

The model that has been used in this work reproduces compressional electromagnetic field fluctuations by a superposition of a large number of propagating Gaussian pulses. In this section we first describe the formulation of a single pulse; we then present the process of randomization and superposition of a large number of such pulses, and finally, we compare the produced model field signatures with real measurements at geosynchronous orbit.

### 3.1 Single pulse

In the spherical coordinate system $(r, \theta, \phi)$ the electric field of a single pulse is given by the following equation:

$$\mathbf{E}_\phi = -\hat{e}_\phi E_0 \left(1+\cos\left(\phi-\phi_0\right)\right)^p \left(\exp(-\xi^2)-\exp(-\eta^2)\right), \quad (1)$$

where $\xi=(r-r_i+v_0t)/d$ determines the location of the maximum value of the incoming pulse and $\eta=(r-2r_i+r_d-v_0t)/d$ determines the location of the reflecting pulse; $r_d$ determines the location where the reflection occurs; $d$ is the radial width of the pulse; $v_0$ is the radial speed of the pulse; $\hat{e}_\phi$ is the azimuthal direction; $E_0$ is the electric field amplitude; $p$ (=1 and 8 in the simulations presented) describes the local time dependence of the electric field amplitude, which is largest at $\phi_0$; and $r_i$ is a parameter in the simulation that determines the arrival time of the pulse. From Eq. (1) the pulse electric field is positive, or westward, for incoming pulses and negative, or eastward, for reflecting pulses, as indicated by the minus sign of the second term in the brackets. The consistent magnetic field of the propagating electric pulse of Eq. (1) is obtained from Faraday's law, after performing the curl calculation of Eq. (1) in spherical coordinates and integrating:

$$B_\vartheta = -\hat{e}_\vartheta \left(\frac{E_0}{v_0}\right)\left(1+\cos\left(\phi-\phi_0\right)\right)^p \left[\left(\exp(-\xi^2)+\exp(-\eta^2)\right)+\left(\frac{d\sqrt{\pi}}{2r}\right)\left(erf(\xi)+erf(\eta)\right)\right] \quad (2)$$

where $erf(x) = {}^2/_{\sqrt{\pi}} \int_0^\infty e^{-x^2} dx$ is the error function.

Each magnetic pulse is superimposed on a background magnetic field, $\mathbf{B}_E$, which is time-independent and is considered a simple dipole field in the present simulation. The pulse field and background field satisfy $\mathbf{E}_\phi \cdot (\mathbf{B}_\theta + \mathbf{B}_E) = 0$ and $\nabla \cdot (\mathbf{B}_\theta + \mathbf{B}_E) = 0$. In the simulation we consider only equatorially mirroring electrons, which move on average according to the relativistic guiding center equation described in (Northrop, 1963):

$$v_d = c\frac{E_\phi \times \mathbf{B}}{B^2} + \frac{\mu c}{\gamma q}\frac{B \times \nabla_\perp \mathbf{B}}{B^2}, \quad (3)$$

where $c$ is the speed of light in vacuum, $\gamma$ is the relativistic correction factor: $\gamma = \left(1-v^2/c^2\right)^{-1/2}$, $\mu$ is the relativistic adiabatic invariant (see Sect. 4.1.1), $\mathbf{E}_\phi$ is the vector electric field, $\mathbf{B}$ is the total magnetic field in the frame of the particle and $\nabla_\perp$ is the gradient perpendicular to the local magnetic field direction and $q$ is the electron's charge.

### 3.2 Multiple pulses

A large number (1200) of random pulses, such as those described in Sect. 3.1, were superimposed; a schematic of the superposition and propagation of the pulses is given in Fig. 1. Each pulse was initiated with a random amplitude $E_0$ in the range from 0.005 mV/m to 0.015 mV/m, a random pulse velocity $v_0$ in the range from 300 km/s to 500 km/s and a random distance $r_i$ in the range from $2{\cdot}10^8$ m to $6{\cdot}10^8$ m, where $r_i$ is a parameter that determines the arrival time of the pulse in the simulation. The radial width of the pulses was kept constant at the value $d$=$4{\cdot}10^8$ m. Angle $\phi_0$ was set to 0°, meaning that all the pulses have a maximum at noon and a null at midnight. A random number generator was used in determining the pulse parameters. One hundred different runs were performed for different random number generator initialization integers ("seeds") and the individual field spectral calculations (see Sect. 4.1.4) as well as the calculations for the electron average squared displacements (see Sect. 4.2) were averaged together.

### 3.3 Comparison of model fields to data

In order to check the validity of the simulation, the model magnetic field was compared against the magnetic field signature at geosynchronous orbit, as measured by GOES-8 on an average (in terms of magnetospheric activity) day. One-minute GOES-8 measurements were used; for this sampling frequency, the Nyquist frequency (and hence the maximum frequency we can monitor in this data set) is 8.3 mHz. To perform the comparison, the Dynamic Power Spectra of the signal time series were calculated, in order to visualize the local time dependence of the ULF fluctuations. This was done by sliding a Hanning window through the data and performing an FFT on the subset of the signal within the window. A 1-day signal includes 1440 data points under a 1-min sampling time; the FFT length of the window was 83 points and there were 79 overlapping FFT blocks in one day's signal in the analysis performed. The frequency resolution in this analysis was 0.2 mHz. An example of the Dynamic Power Spectral Density of one day's GOES-8 data is shown in the left panel of Fig. 2. In this figure, the field variation in the ULF regime is plotted in the top panel, and the power spectral density in the lower panel. The field variation is calculated by subtracting the large-scale variation (e.g. diurnal variation and other large-scale changes) from the original signal; the large-scale variation is calculated using a wavelet signal decomposition scheme, with a Daubauchies wavelet and 25 coefficients (for a review see, e.g. Rioul, 1991). In this day, most of the fluctuations are in the z-direction (indicating compressional fluctuations); it is also a day with a smooth diurnal variation, without any indications of multiple processes going on at the same time.

In order to place the magnetospheric fluctuations of the selected day shown in the left panel of Fig. 2 in the context of the average behaviour of the magnetosphere, a survey of the average Dynamic Power Spectra of ULF magnetic field fluctuations has been conducted, using 8 years of geosynchronous magnetic field measurements from GOES-8 satellite. In this survey, daily calculations of the Dynamic Power Spectra of the magnetic field, computed in exactly the same manner as described above, were averaged together. The averaging was performed for two cases: in one case the Dynamic Power Spectra from all days were used; in the second case only the days with a daily mean $|Dst|$ value of less than 20 were used. The study has shown that the selected day has ULF power that is one order of magnitude less than the average power of all days of the 8 year survey; the ULF power of the selected day is of the same order of magnitude with the average power from all days, with a daily mean $|Dst|$ value of less than 20.

The signatures produced by the model propagating pulses were recorded at geosynchronous orbit using the same sampling frequency as GOES-8 measurements, so that the model fluctuating fields could be compared to the data. The spacecraft's motion around the Earth was also simulated. The modelled magnetic perturbation signal and its dynamic power spectrum are shown in the right panel of Fig. 2, keeping the same format as in the left panel. From the comparison of the upper panels of the two figures we note that there is low-frequency fluctuation in the midnight region in the GOES-8 data, contrary to the model; however, these fluctuations are below the 1.5 to 10 mHz range of ULF fluctuations that are of interest in this study. In general, the model manages to reproduce in a realistic way the power contained in the Pc-5 fluctuations of the magnetic field at geosynchronous orbit for this particular day.

## 4 Radial Diffusion Coefficients

In this section the effect of the model field fluctuations on a set of energetic electrons of a single $\mu$-value is explored, as it is expressed by the diffusion coefficient $D_{LL}$. The expressions for the magnetic diffusion coefficient are first described, as they were formulated by Falthammar (1965) and generalized by Fei et al. (2006), and the various terms involved are discussed. We then show the results from test-particle simulation in a background dipole magnetic field with superimposed field fluctuations, and we calculate numerically the diffusion coefficient $D_{LL}$. Based on the model characteristics and on the discussion in Falthammar (1965), we relate the simulated diffusion coefficient to $D_{LL}^{B,Sym}$, the symmetric magnetic diffusion coefficient.

### 4.1 Theoretical estimates of the radial diffusion coefficient

The diffusive transport of electrons in the radiation belts can be described by the Fokker-Plank equation which describes the evolution of phase-space-density in terms of the three

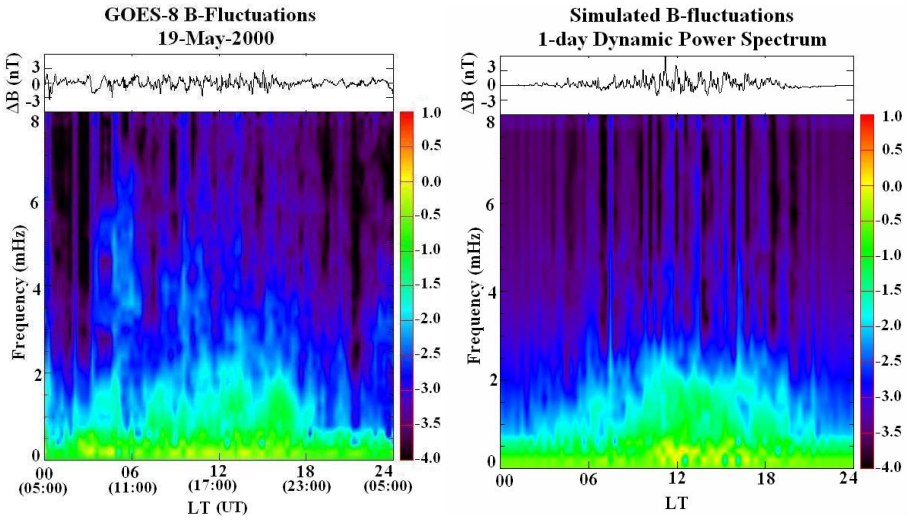


**Fig. 2.** Comparison of one day of GOES-8 magnetic field measurements with one day of simulated model magnetic field. On the upper left panel the diurnal large-scale variation has been subtracted from the data using wavelet decomposition, to reveal the fluctuation level in the ULF regime. On the lower panel, color-coded is the power of the magnetic field signal as a function of frequency and time (dynamic power spectrum); the units in the color scale correspond to the logarithm of the power, in $nT^2$/Hz. The fluctuations and the spectra of the magnetic field are plotted in time for 24 h from 05:00 UT, when GOES-8 is located at midnight, to 05:00 UT of the next day. On the right-hand side, the model magnetic field is recorded at geosynchronous orbit with the same time resolution and duration as the GOES-8 measurements. Spacecraft motion around the Earth is also simulated. An azimuthal amplitude modulation of: 1+cos($\phi$) was used in this simulation.

adiabatic invariants of the electrons (Schulz and Lanzerotti, 1974; Bourdarie et al., 1997). When the first two adiabatic invariants are conserved but the third one is violated, the resulting expression is the radial diffusion equation, expressed as:

$$\frac{\partial F}{\partial t} = L^2 \frac{\partial}{\partial L}\left(\frac{D_{LL}}{L^2}\frac{\partial F}{\partial L}\right), \tag{4}$$

at constant first adiabatic invariant $\mu$ and second adiabatic invariant $J$. In Eq. (4), $F$ is the electron phase space density and is related to the more experimentally familiar quantity $j$, the electron differential flux, by: $F=j/p^2$, where $p$ is the electron momentum. The radial diffusion coefficient, $D_{LL}$, is obtained by integrating the instantaneous rate of change of the shell parameter $L$ for a large number of particles, over an interaction time $\tau >> 2\pi/\Omega$, where $\Omega$ is the particle drift frequency:

$$D_{LL} \equiv \frac{\langle (\Delta L)^2 \rangle}{2\tau}. \tag{5}$$

In the above expression, the brackets denote integration over time $\tau$, and $\Delta$ denotes an average over a large number of particles [see also Schultz and Lanzerotti, 1974, pp. 89–92].

The magnetic diffusion coefficient, $D_{LL}^{B,Sym}$, produced by electromagnetic fluctuations on particles of a single $\mu$-value that are drifting in a symmetric background magnetic field, has first been derived theoretically by Falthammar (1965). This derivation is non-relativistic and includes only single-mode fluctuations of mode number $m$=1. Recently, Fei et al. (2006) generalized Falthammar's expression to include relativistic electrons and multiple mode numbers of fluctuation. The expression they derived has the following form:

$$D_{LL}^{B,Sym} = \frac{\mu^2}{8q^2 B_E^2 R_E^4}\left(\frac{L^4}{\gamma^2}\right)\sum_{m=1}^{\infty} m^2 P_m^B(m\omega_d). \tag{6}$$

In the above equation $\mu$ is the value of the first adiabatic invariant of the electrons considered, $q$ is the electron charge, $\gamma$ is the Lorentz relativistic factor, $B_E$ is the magnetic field strength at the surface of the Earth, $R_E$ is one Earth radius, $m$ is the azimuthal mode number of the fluctuation and $P_m^B(\mathrm{m}\omega_d)$ is the power spectral density of the compressional wave magnetic field at frequency $m$-times the drift frequency $\omega_d$ of the electrons considered. The summation is performed from $m$=1 to infinity for all participating modes. In the following we comment on some of the terms in Eq. (6): the first adiabatic invariant $\mu$, the Lorentz relativistic factor $\gamma$, the mode number of fluctuation $m$, and the power spectral density $P_m^B$ at frequency $m\omega_d$.

#### 4.1.1 First adiabatic invariant, $\mu$

In Eq. (6), $\mu$, the relativistic adiabatic invariant associated with the electrons' gyro-motion, can be written as: $\mu = p_\perp^2 / 2m_0 B$, where $p_\perp$ is the electron's perpendicular momentum, $m_0$ is the electron rest mass and $B$ is the magnetic field strength. Particles of a single $\mu$-value will have different energies at different $L$, since the kinetic energy is proportional to the magnetic field strength and decreases with

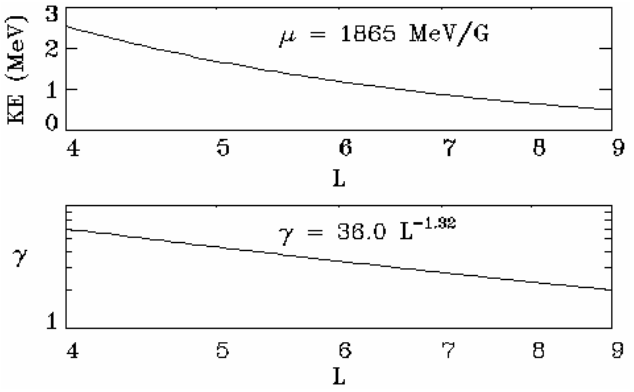


**Fig. 3.** Upper panel: Kinetic energy of electrons as a function of $L$ for a single first adiabatic invariant, $\mu$=1865 MeV/G. Lower panel:$L$-dependence of $\gamma$ the Lorentz relativistic correction factor, for $\mu$=1865 MeV/G.

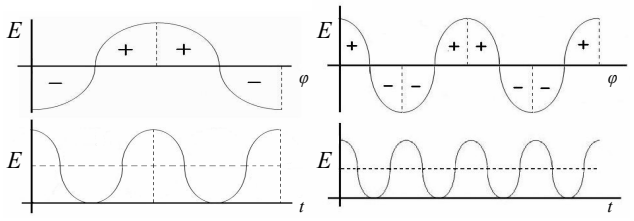


**Fig. 4.** In the upper panels, the amplitude of the ULF perturbation electric field is given as a function of the azimuthal angle $\phi$ for idealized $m$=1 (left panel) and $m$=2 (right panel) poloidal modes of fluctuations. In the lower panels, the amplitude of the electric field that a particle experiences while drifting at a frequency $\omega_D$=m$\omega$ is given as a function of time.

increasing $L$. The Kinetic Energy ($KE$) versus $L$ relation for the $\mu$-value used in the simulation, $\mu$=1865 *MeV/G*, is given in the upper panel of Fig. 3. This $\mu$-value corresponds to electrons of energy 2.5 *MeV* at $L$=4.0, 1 *MeV* at $L$=6.6, and 0.7 *MeV* at $L$=8.0.

### 4.1.2 Lorentz relativistic factor, $\gamma$

The Lorentz relativistic correction factor $\gamma$ can be expressed as: $\gamma = (KE + m_0c^2)/m_0c^2$, where $KE$ is the electron's kinetic energy, $m_0$ is the electron rest mass and $c$ is the speed of light. As mentioned above, for particles of a single $\mu$-value the kinetic energy decreases with increasing $L$. From the $KE$-versus-$L$ relation and from the expression for $\gamma$ we can calculate the $\gamma$-versus-$L$ relation. For the electrons traced in the simulation, which have a $\mu$-value of 1865 *MeV/G*, the $L$-dependence of the Lorentz factor is plotted in the lower panel of Fig. 3 and can be approximately fitted as: $\gamma = 36 \cdot L^{-1.32}$. In the non-relativistic case, $\gamma$ is equal to one at all $L$; in the ultra-relativistic limit, $\gamma$ is proportional to $L^{-1.5}$ and the factor $L^4/\gamma^2$ in Eq. (6) is proportional to $L^7$.

### 4.1.3 Mode number of compressional ULF fluctuations, $m$

Theoretically, the fluctuating electric field of the Earth along the equatorial plane at any given time $t$ could be approximated by an expansion of a Fourier series of the form (similarly for the magnetic field):

$$E(t,\phi) = \tfrac{1}{2}E_0(t) + \sum_{m=1}^{\infty} a_m(t) \cdot \cos(m\phi) + \sum_{m=1}^{\infty} b_m(t) \cdot \sin(m\phi) \quad (7)$$

In this expansion, $m$ describes the mode of fluctuation of each component in the generalized Fourier series; $\alpha_m(t)$ and $b_m(t)$ are the time-dependent coefficients of the fluctuating electric field, and $E_0$(t) describes the global oscillations of the magnetosphere (global compressions and relaxations), corresponding to mode number $m$=0. We note here that the $m$=0 mode of global oscillations is not included in the sum of Eq. (6), since it does not contribute to particle radial diffusion: global fluctuations of the magnetic field will cause a fluctuation in the radial distance of a particle, however, the net radial displacement of the particle averaged over a time period much longer than the particle's drift period will be zero, as long as there is no net increase or decrease in the global magnetic field intensity. In contrast, the non-zero modes of fluctuations can produce a net radial displacement to some particles, by what has been described as enhanced radial transport (diffusion) by drift resonance.

The concept that an energetic particle undergoing a periodic azimuthal drift at a particular drift frequency $\omega_d$ around the Earth can experience a resonant acceleration, due to the interaction with electric field perturbations that do not average to zero over the particle's drift orbit, has been recognized early on in magnetospheric physics (Dungey, 1964). This resonant condition has been expressed as:

$$\omega - m\omega_d = 0, \quad (8)$$

where $\omega$ is the frequency of the field perturbations, $\omega_d$ is the drift frequency of the particle and $m$ is the azimuthal mode number. The drift resonance of particles with fluctuating fields is demonstrated in Fig. 4, which gives a schematic of the azimuthal and temporal characteristics of a fluctuating monochromatic electric field for two cases, corresponding to an idealized poloidal $m$=1 (left panels) and $m$=2 (right panels) mode of perturbation, respectively. In the left panels of Fig. 4, the perturbation is modulated by a $cos(\phi)$ function, whereas in the right panels the perturbation is modulated by a cos($2\phi$) function. In the upper panels of Fig. 4, the amplitude of the electric fields is plotted versus the azimuthal angle $\phi$ for one time instance $t_0$. The electric field in both plots points in the azimuthal direction, with eastward (westward) being positive (negative). The lower panels of Fig. 4 show the drift-resonant interaction of a particle drifting with a frequency $\omega_d$ around the Earth with an electric field perturbation at the same frequency, $\omega$=$\omega_d$, for an $m$=1 mode (left panel), and twice the drift frequency, $\omega$=2$\omega_d$, for an $m$=2 mode of fluctuation (right panel). The net electric field that

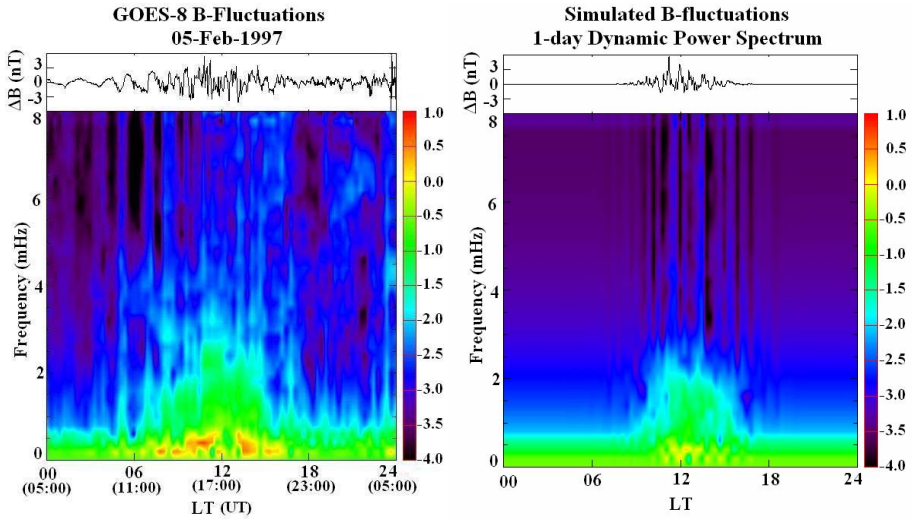


**Fig. 5.** Comparison of one day of GOES-8 magnetic field measurements with one day of simulated model magnetic field. The selected day has ULF fluctuation activity more localized around noon, compared to Fig. 2. The panel layout is similar to Fig. 2. On the right-hand side, the azimuthal amplitude modulation is governed by an $(\cos(\phi)+1)^p$ azimuthal dependence, with $p$=8, producing pulses that are more localized around noon.

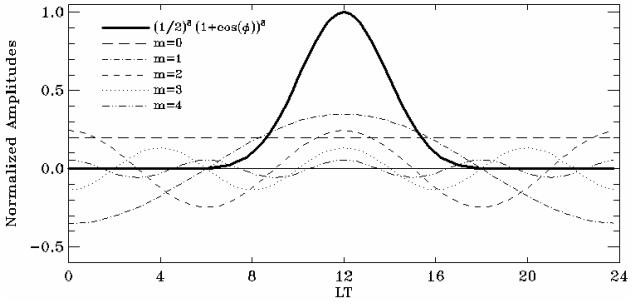


**Fig. 6.** The azimuthal modulation of the earthward pulses by the factor $1+\cos(\phi)^8$ is given by the solid thick line, as a function of local time. The rest of the lines give the azimuthal modulation of the first five modes of fluctuation, as marked.

the electron would experience along its drift path is non-zero for both cases, and hence the average work $\dot{W}=q\mathbf{E}\cdot\mathbf{V}$ done by the electric field on the particle of speed $\mathbf{V}$ is also non zero.

In our model the amplitude of the fluctuating field follows an azimuthal modulation of the form $(1+\cos(\phi-\phi_0))^p$, which introduces a smooth transition from maximum fluctuations at noon (angle $\phi_0$) to zero fluctuations at midnight (angle $\phi_0-\pi$). The particular amplitude modulation was selected in order to match the spectral features that are commonly observed in the radiation belts, which show enhanced fluctuations at noon. The exponent $p$ determines the extent of the azimuthal dependence: a large $p$-exponent creates a modulation that confines the pulses around $\phi$=0. Two simulations are presented: in the first simulation an exponent of $p$=1 is used, which introduces an $(1+\cos(\phi))$ amplitude modulation. The distribution of power of the model fluctuations in local time is given by the dynamic power spectra in the right panel of Fig. 2; in the same plot, the model fields are compared to measurements made on 19 May 2000 by GOES-8 spacecraft at geosynchronous orbit. A comparison with Eq. (6) shows that this amplitude modulation includes contributions from the $m$=0 global mode and the $m$=1 mode of ULF perturbations. As mentioned above, the $m$=0 mode of global oscillations does not contribute to particle radial diffusion; hence we will refer to this simulation of field perturbations as single-mode simulation.

In the second simulation performed, an exponent $p$=8 was used, modulating the azimuthal dependence of the fluctuating fields as $(1+\cos(\phi))^8$. This modulation creates a compressional perturbation that is azimuthally localized around noon. The distribution of power of the model fluctuations in local time is given by the dynamic power spectra of the right panel of Fig. 5. Such azimuthal localizations in the fluctuating fields are commonly observed: an example is given in the left panel of Fig. 5, which shows magnetic field measurements made by GOES-8 satellite on 5 February 1997. The format of the plot is similar to Fig. 2, with noon corresponding to the center of the plots and midnight to the edges of the plots. In order to determine which modes are included in the simulated perturbations of Fig. 5, and also in order to find the power at each mode, the azimuthal dependence factor $(1+\cos(\phi))^8$ can be expanded as follows:

$$\begin{aligned}\left(\tfrac{1}{2^8}\right)(1+\cos(\phi))^8 &= 0.2+0.35\cos(\phi)+0.24\cos(2\phi)\\ &+0.13\cos(3\phi)+0.06\cos(4\phi)+\\ &+0.017\cos(5\phi)+0.0036\cos(6\phi)\\ &+0.0005\cos(7\phi)+0.00003\cos(8\phi)\end{aligned} \quad (9)$$

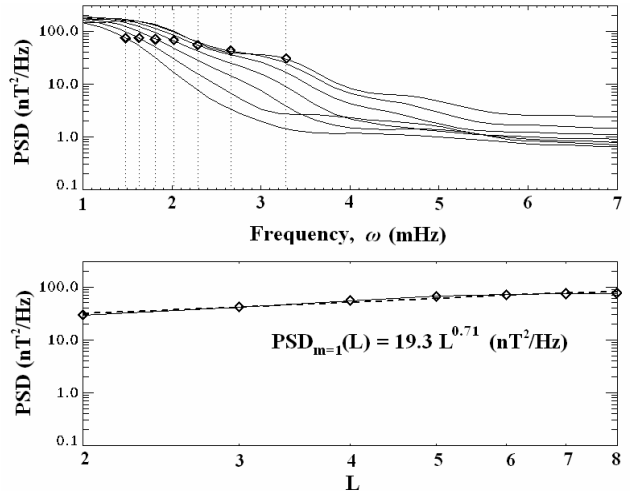


**Fig. 7.** Top: The Power Spectral Density of the fluctuating fields in the single-mode simulation ($m$=1) is plotted with solid lines for various $L$ from $L$=2 to $L$=8 as a function of frequency $\omega$ (in mHz). The highest line corresponds to $L$=2. The diamonds correspond to the power of fluctuations at frequency $\omega_d$ (drift frequency of electrons of $\mu$=1865 MeV/G) at the particular $L$. The power at these $L$ is plotted in the lower panels as a function of $L$; a fit through these points gives the $L$ dependence function, PSD$_{(}m$=1($L$)).

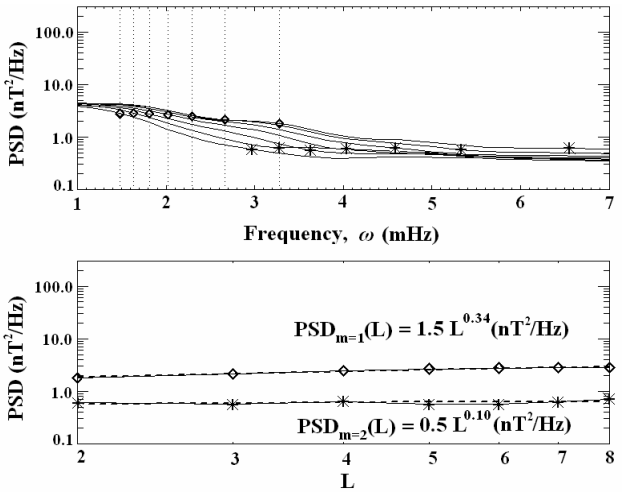


**Fig. 8.** The power of fluctuations for the multiple-mode simulation ($m$=1 to $m$=8) is plotted in a similar fashion. The diamonds correspond to fluctuations at frequency $\omega_d$; the asterisks correspond to fluctuations at frequency 2 $\omega_d$.

The constant term in the expansion represents an $m$=0 global mode of oscillation, which does not contribute to radial diffusion since it does not satisfy the resonance condition stated in Eq. (8). A comparison of Eq. (9) with Eq. (7) shows that there are nine modes of fluctuation in the model fields, with mode numbers from $m$=0 to $m$=8. Figure 6 gives a graphical representation of the relative contribution of each term in Eq. (9). In this figure, the thick solid line marks the azimuthal dependence of factor $(1+\cos(\phi))^8$, which modulates azimuthally all pulses in the simulation, producing a maximum at noon. The thinner lines give the azimuthal dependence of the various contributing modes of fluctuation as marked. The various terms are normalized, so that the sum of the amplitudes of all modes is one at noon.

It should be noted that, in the magnetospheric perturbations recorded on 19 May 2000 and 5 February 1997, multiple modes of fluctuations of higher mode numbers might coexist at the same time, contributing to the total spectra in the left panels of Figs. 2 and 5; these cannot be distinguished from single-satellite measurements. However, in these particular days, most of the magnetic field fluctuations were found in the $B_z$ (northward) component; we speculate that they mostly correspond to quiet-time compressional fluctuations of the magnetopause, caused by solar wind variations, which are usually related to low-$m$ modes of fluctuations. Hence we find it reasonable to assume that most of the power contributing to radial diffusion in these days would be concentrated in the lowest mode numbers of fluctuations.

#### 4.1.4 Power spectral density of ULF electromagnetic perturbations

The analytic expressions of the model fluctuating fields make possible the numeric calculation of the power of the fluctuations as a function of frequency and time at various $L$; the calculations of the PSD that an electron drifting in a dipole field would experience at different $L$ are plotted in the upper panels of Figs. 7 and 8 as solid lines, one for each $L$, from $L$=2 to $L$=8. Fig. 7 corresponds to the single-mode simulation, whereas Fig. 8 corresponds to the multiple-mode simulation.

We are only interested in the power that will contribute to an electron's radial transport, through the drift-resonant effect of the ULF perturbations that was described above. The drift-resonant effect has been included in Eq. (6) of the diffusion coefficient $D_{LL}^{B,Sym}$ as contributions to radial diffusion only from fluctuations at frequencies $m\omega_d$. Thus, the total PSD contributing to radial diffusion can be expressed for multiple modes of fluctuations as:

$$PSD = \sum_{m=1}^{\infty} m^2 P_m^B(m\omega_d), \tag{10}$$

where PSD is measured in $T^2$/Hz, $m$ is the mode number of the ULF wave component and $\omega_d$ is the drift frequency of the electrons considered. In the simulations performed only particles of a single $\mu$-value were traced; for this $\mu$-value the electron energy that corresponds to each $L$ was plotted in the upper panel of Fig. 3. From the energy-versus-$L$ relationship for this particular $\mu$-value we can obtain the particle drift frequency at a particular $L$. In the upper panels

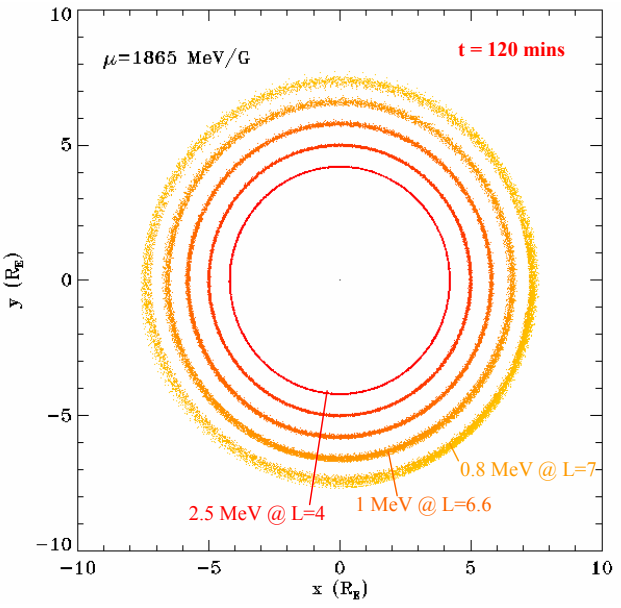


**Fig. 9.** In the simulation particles of $\mu$=1865 MeV/G were initialized in rings at various $L$. Particle locations are plotted after 2 h of interaction with the fluctuating fields. Particle energy is color-coded, with inner particles (red) having highest energy.

of Fig. 7 and 8 we plot vertical dotted lines at the drift frequencies $\omega_d$ of electrons at various $L$, from $L$=2 to $L$=8, for $\mu$=1860 MeV/G. The power at each frequency $\omega_d$ is marked as a diamond. In Fig. 8, where the power of multiple-mode fluctuations is plotted, we also mark the power at frequencies $2\omega_d$ corresponding to mode number $m$=2 with asterisks. In the lower panels of Fig. 7 and 8 we plot the power at each frequency $\omega_d$ as a function of the $L$-value corresponding to that frequency, also with a diamond; similarly, we mark with asterisks the power at frequencies $2\omega_d$. Thus, there is a one-to-one relation between the asterisks and diamonds of the upper and lower panels of Figs. 7 and 8. We then perform a fit through the points in the lower panels of Figs. 7 and 8, and obtain the power-versus-L relationship for the $m$=1 case in Fig. 7, and the $m$=1 and $m$=2 cases in Fig. 8. A similar process is followed for the higher mode numbers for the multiple-mode simulation, which are not plotted here.

For the single-mode simulation the Power Spectral Density as a function of $L$ is found to be:

$$P^B_{m=1}(\omega_d) = 19.3 \cdot L^{0.71} (nT^2/Hz) \tag{11}$$

For the multiple-mode simulation, Table 1 gives an overview of the contribution to radial diffusion from the participating modes. The mode number $m$ is given in the first column; the relative power contribution from each mode, $\beta_m$, is given in the second column by the square of the normalized amplitude of each mode, which is the coefficient of each sine term in Eq. (9); and the relative contribution to the diffusion coefficient is given in the third column, by multiplying $\beta_m$ by $m^2$,

**Table 1.** The relative contribution of the participating modes to the diffusion coefficient.

| m | $\beta_m$ | $m^2$ $\beta_m$ | $P^B_m$ [$nT^2$/Hz] |
|---|---|---|---|
| 0 | 0.04 | 0.0 | 0 |
| 1 | 0.12 | 0.12 | $52*L^{1.11}$ |
| 2 | 0.06 | 0.23 | $11*L^{-0.03}$ |
| 3 | 0.017 | 0.15 | $10*L^{-0.44}$ |
| 4 | 0.0036 | 0.058 | $26*L^{-1.26}$ |
| 5 | 0.00029 | 0.0073 | $32*L^{-1.42}$ |
| 6 | 0.000013 | 0.00047 | — |
| 7 | 0.00000025 | 0.000012 | — |
| 8 | 0.0000000009 | 0.000000058 | — |

as indicated by Eq. (10). In the last column, the power spectral density $P^B_m$ is given as a function of $L$ for each mode, calculated as described above. In Table 1, calculations of $P^B_m$ for the $m$=6, 7 and 8 cases have been excluded, since they required calculation of the power of fluctuations at 6, 7 and 8 times the particles' drift frequencies, respectively, which is well beyond the Pc-5 range of fluctuations that has been simulated by the pulse model. However, the contribution of these modes to radial diffusion is insignificant, as is discussed below.

In order to calculate the theoretical diffusion coefficient, by substituting $\mu$=1865*MeV/G*, $\gamma$=$36 \cdot L^{-1.32}$, $B_0$=0.31 Gauss and $R_E$=$0.6371 \times 10^7 m$, Eq. (6) can be written as:

$$D^{B,Sym}_{LL} = 5.77 \cdot 10^6 \cdot L^{6.64} \cdot \Sigma m^2 P_B(m\omega_d). \tag{12}$$

For the single-mode case, from Eqs. (12) and (11) we obtain:

$$D^{B,Sym_{(m=1)}}_{LL} = 5.5 \cdot 10^{-11} \cdot L^{7.35}. \tag{13}$$

For the multiple-mode simulation, from Eq. (12), using the expressions from the last column of Table 1 for the various $P^B_m$ terms, we get:

$$D^{B,Sym_{(m=1..8)}}_{LL} = \Big(1.8 \cdot L^{7.75} + 0.7 \cdot L^{6.61} + 0.4 \cdot L^6.2 + 0.4 \cdot L^5.4 + \ldots\Big) \cdot 10^{-11}. \tag{14}$$

### 4.2 Numerical calculation of $D^{B,Sym}_{LL}$ from test-particle simulation

In the approach presented herein, we calculate numerically the diffusion coefficient $D^{B,Sym}_{LL}$ that corresponds to electromagnetic symmetric radial diffusion by the actual radial displacement of the electrons: we trace the drift orbits of relativistic electrons as they are moving under the effect of the fluctuating magnetic and electric fields in the equatorial plane of a dipole field by integrating Eq. (3), and we monitor their radial displacement in time. In order to calculate

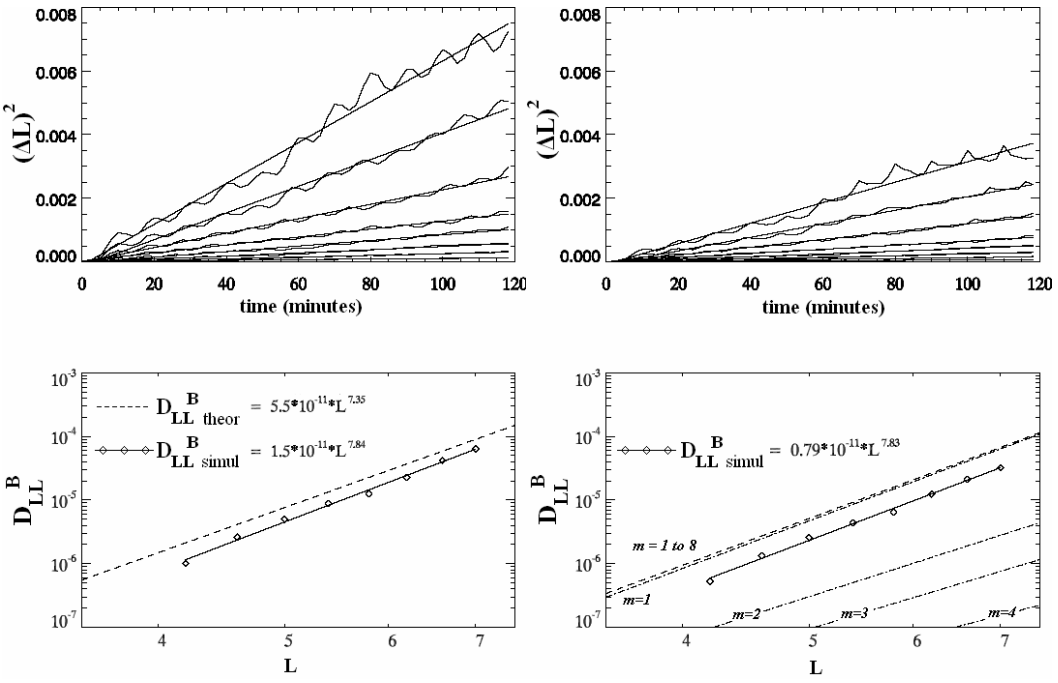


**Fig. 10.** In the upper panels, each line represents the time evolution of the average squared displacement, $(\Delta L)^2$, of particles evenly distributed in rings at various $L$ from 4.6 (smallest slope) to 7.0 (largest slope), every L=0.4. The fit to each line gives the rate of change of $<(\Delta L)^2>$ from which the radial diffusion coefficient at $L$ is calculated. On the left (right) panels, diffusion rates are calculated for the single-mode (multiple-mode) simulations. In the lower panels, the radial diffusion coefficients at the various $L$ are plotted as diamonds. The fit through these points (solid line) gives the $L$-dependence of $D_{LL}^{B}$, in units of 1/s. The theoretical estimate for the diffusion coefficient is drawn with a dashed line both in the left plot for the single-mode simulation, and in the right plot for the multiple-mode simulation. In the multiple-mode simulation the contribution to the radial diffusion coefficient from the first four modes is plotted with dashed-dotted lines.

$D_{LL}^{B,Sym}$ as a function of $L$ we initialize rings of electrons at various $L$, from $L$=4.6 to $L$=7.0 every dL=0.4, across all local times. We monitor the electrons under the effect of the fluctuating fields at each ring with a 2 min resolution. The positions of the rings' electrons after 2 h simulated time are shown in Fig. 9. In this figure the electron energy is color-coded. It can be seen that there is an $L$-dependence of the diffusion rates, with electrons at larger $L$ diffusing more than electrons at lower $L$. The diffusion coefficient at the particular $L$ is then calculated from the slope of the average squared displacement, $(\Delta L)^2$, of a large number of electrons, as described by Eq. (5). In the upper panels of Fig. 10, the simulated $(\Delta L)^2$ from electron tracing is plotted as a function of time for the selected $L$ values, together with the corresponding linear fits. The left (right) panel corresponds to electrons under the effect of the single-mode (multiple-mode) fluctuations that were described above. In both simulations a periodicity can be observed in the rate of change of $(\Delta L)^2$; this is further discussed in the next section.

In the lower panels of Fig. 10 we plot the value of the simulated diffusion coefficient, determined by the slope of each of the lines of the upper panels, as diamonds, at the particular $L$ of the corresponding particle ring. The expression for the simulated $D_{LL}^{B,Sym}$ as a function of $L$ is then calculated from a linear fit through these points, and it is plotted as a solid line in the lower panel of Fig. 10. The expression for $D_{LL}^{B,Sym}$ in this plot is given in units of 1/s. For comparison, in the lower panels of Fig. 10 we also plot the theoretical expression for $D_{LL}^{B,Sym}$ given by expressions (13) and (14), as described in Sect. 4.1.4, for the left and right plots, respectively. For the single-mode simulation, the theoretical $D_{LL}^{B,Sym}$ is plotted with a dashed line in the lower left panel. For the multiple-mode simulation, the various terms contributing to $D_{LL}^{B,Sym}$ are plotted in the lower right panel of Fig. 10 with dashed-dotted lines for the first four mode numbers; each line corresponds to one of the terms in expression (14). In the same plot, the total theoretical $D_{LL}^{B,Sym}$ is plotted with a dashed line. It can be seen from this plot that the $m$=1 mode contributes mostly to the total symmetric diffusion coefficient. From the comparison between the simulated and theoretical diffusion coefficients, an offset by a factor of $\sim$2 can be distinguished for both simulations; this is further discussed in the next section.

## 5 Discussion

The model of magnetospheric variability that has been presented simulates compressional ULF poloidal fluctuations; due to the random initialization and propagation speeds of a large number of pulses, the model exhibits broadband spectral characteristics, with ULF power distributed in a broad range of ULF frequencies. Physically, this model can be considered to simulate the initial phase of the temporal development of the ULF excitation (e.g. Radoski, 1976; Wright, 1994): during this phase, an initially purely compressional perturbation caused by magnetopause instabilities or by solar wind pressure pulses propagates inward in the magnetosphere and is reflected at the plasmapause, due to the large gradient in the Alfvén velocity.

The radial diffusion coefficient calculated through this model was compared to theoretical calculations of $D_{LL}^{B,Sym}$, the radial diffusion coefficient due to electromagnetic perturbations in a symmetric (dipolar) background field. The theoretical calculation of $D_{LL}^{B,Sym}$ by Falthammar (1965) can only be applied to non-relativistic particles, and thus cannot be compared to our results; however, the recent generalization by Fei et al. (2006) of Falthammar's diffusion coefficient includes relativistic particles and contributions from all participating modes. We compared the radial diffusion coefficient between theory and the numerical simulations for both a broad azimuthal extent, simulating an $m$=1 mode, and a more localized azimuthal extent that mimics multiple, higher-$m$ modes of compressional fluctuations. The comparison has shown that the $L$-dependence of the diffusion coefficient (i.e., the slope of $D_{LL}^{B}$ as a function of L) from particle tracing is in agreement with the slopes from the theoretical estimates for both simulations; however, the numerical calculations of the diffusion coefficient are lower than the theoretical estimates by approximately a factor of two, consistently for both simulations. In the following discussion, a speculation on the reason for the factor-of-two discrepancy is presented; we note, however, that at this point a conclusive argument cannot be provided.

The speculation for the discrepancy by a factor of $\sim$2 involves correctly counting only geoeffective waves when calculating the PSD from expression (10). In the theoretical formulation of the diffusion coefficient by Falthammar (1965) and Fei et al. (2006) only waves that propagate in the same direction of the electron drift will resonantly interact with the electron and accelerate it, assuming they have the appropriate frequency, as discussed above. This has been demonstrated by Elkington et al. (2003), who have shown that, in the case of a global westward propagating wave, opposite to the direction of electron drift, the net energization seen over the course of the orbit integrates to zero. In the following description, waves moving in the same direction as the eastward gradient drifting electrons will be described as having "negative" frequency; those moving in the opposite direction will be described as having "positive" frequency.

Contrary to the above description of the waves with westward (positive) and eastward (negative) frequency components, the pulse fields in the simulation propagate radialy inward and outward; however, due to the imposed azimuthal modulation they include points of no displacement, or nodes, in their azimuthal extent, always at the same azimuthal location along the medium. This, in general, is a characteristic of standing wave patterns. Standing waves are produced whenever two waves of identical frequency interfere with one another while traveling in opposite directions along the same medium. Thus, the ULF waves in the simulation can be considered to correspond to a positive and a negative wave component, of which only the negative will contribute to enhanced radial diffusion, which means that only one-half of the power of the field fluctuations should be included in the expression (6) for the radial diffusion coefficient. Thus, calculating the diffusion coefficient based only on the spectral characteristics of the waves without knowledge of the actual wave geometry and propagation direction can yield incorrect results. The numerical tracing of the particle drift orbits correctly captures the particle interactions with the given fluctuating fields and gives an accurate calculation of the diffusion coefficient; however, when simulating realistic field fluctuation more information on wave geometry is needed, from multiple spacecraft and from polarization analysis of the wave measurements. In order to address this subject with more conclusive arguments, the pulsations in the simulation could be decomposed into westward and eastward propagating pulsations and the individual effects of each propagation direction could be quantified; however, this is beyond the scope of the present work.

It should be emphasised that the comparison between the rates of particle radial transport calculated from the test-particle simulation and those predicted by the theoretically derived diffusion coefficients cannot be generalized and will not yield similar results under all magnetospheric conditions. In general, the use of a linearized theory to describe the radial displacement of particles by randomly varying fields that violate the third adiabatic invariant is based on the assumption of small disturbances, in which case the particle orbits deviate only slightly from following constant-B contours. Test-particle simulations performed in other studies have yielded radial transport processes that vary significantly from being diffusive. For example, the test-particle simulations of Riley and Wolf (1992), which focused on storm events, have shown mediocre agreement with radial diffusion estimates; similarly, the simulation in Ukhorskiy et al. (2006), which used a fluctuating dynamic pressure as input to a dynamic magnetospheric model, has also shown a deviation from a linearized behaviour of the radial transport process. An extreme example is the test particle simulation of the March 1991 storm by Li et al. (1993), in which the short time scale of the large variation in the solar wind induces an electric field which reconfigures the whole dayside magnetosphere

and radialy transports particles deep in the magnetosphere, in a radial transport process that is fundamentally different from diffusion. The model that was presented can be used to simulate energetic particle radial transport in both quiet magnetospheric conditions, such as are modelled herein, as well as in more intense magnetospheric conditions, where the radial transport processes cannot adequately be described as diffusive. Furthermore, through a comparison of the two approaches, such as was presented herein, the limits of the levels of magnetospheric ULF fluctuations under which the theoretically derived radial diffusion coefficients can be applied to approximate radial transport processes could be quantitatively defined.

In the upper panels of Fig. 10 a periodic oscillation of the average squared displacement of the particles in each particle ring can be observed; to determine the period of the oscillation, an FFT was performed on the slopes of Fig. 9 that show the periodic oscillations. It was found that these oscillations have periods ranging from 8 min at 4.6 RE to 10.2 min at 7.0 RE, corresponding to the drift periods of the $\mu$ = 1865 MeV/G particles at the various rings. In order to rule out phase-bunching effects which might arise due to a preferential interaction of particles of the appropriate phase with any individual sequence of pulsations, 100 different runs with different random number generator seeds (and hense different sets of random pulses) were performed, and the resulting slopes were averaged together, as described in the paper in Sect. 3.2. A consideration for the particular behaviour involves the interaction of the particles within each ring with the broadband fluctuations of mode number m=0, the global azimuthal mode, which coexists with the m=1 pulsations in the first simulation, and with the m=1 to m=8 pulsations in the second simulation. In this consideration, any given monochromatic pulsation of mode m=0 would cause a periodic adiabatic radial displacement and corresponding energization of each particle at the monochromatic pulsation's frequency, which would correspond to a periodic change in $(\Delta L)^2$ at the same frequency. For a broadband fluctuation, such as that acting on the particles in these simulations, energetic particles respond preferentially to the field fluctuations with frequencies comparable to their drift frequencies. This effect is consistent with radial diffusion, and has been discussed in Schultz and Lazerrotti (1974) (pp. 152–159). A detailed investigation of such effects of broadband, m=0 fluctuations, acting on single-energy particles is currently being conducted and will be reported in the near future.

In the presented simulations, only particle diffusion in fluctuations in a symmetric background magnetic field was considered. The diffusion coefficients in an asymmetric background magnetic field, $D_{LL}^{B,\mathrm{Asym}}$, behave in a different manner: they have different resonant frequencies, they are also proportional to the square of the asymmetric factor $\Delta B/B_E$, and have a steeper $L$-dependence. Also, as noted by Fei et al. (2006), symmetric resonance mode dominates the radial diffusion process in the inner and middle $L$-region, whereas asymmetric resonances are more important in the outer $L$-region; thus, a similar simulation with identical fluctuating fields to the ones presented should be carried out under an asymmetric background field in order to calculate the total diffusion coefficient due to poloidal fluctuations, using both the symmetric and the asymmetric terms.

The mode number of the observed fluctuations cannot be determined conclusively by single-satellite measurements, as in general $2m$-satellite measurements are needed to determine pulsations of mode number $m$. Thus, two-satellite measurements can indicate the amount of power in mode $m$=1, four-satellite measurements can indicate the power in mode $m$=2, etc. However, most of the storm-time, compressional pulsations that are observed at noon are global pulsations with low azimuthal mode numbers, making the selection of modes in the simulations realistic.

In the model the pulses propagate at velocities that are assumed to remain constant and also retain constant amplitude, both during the pulses' inbound propagation and after reflection at the inner boundary. Instead, Mathie and Mann (2001) have shown that there is an exponential decay of 1–10 mHz Pc-5 ULF wave power with decreasing $L$-shell, the decay increasing with solar wind speed, indicating a stronger dependence of pulsation power on higher $L$-shells, in the region $L$= 3.8–6.8. Furthermore, within the magnetospheric cavity the compressional perturbations that this model simulates propagate with the speed of a fast mode, magnetosonic wave, which would be approximately equal to the Alfvén speed in the Earth's magnetosphere, since the ion acoustic wave speed is very low. Thus, in order to better represent the propagation and decay characteristics of the disturbances in the magnetosphere, a variable speed could be introduced to the propagating pulses. Perturbations that follow the Alfvén speed profile in the Earth's magnetosphere are expected to accelerate as they propagate from the magnetopause to the inner magnetosphere until being reflected at the plasmapause due to the large gradient in the Alfvén speed; such a radial velocity profile calculated through numerical models has been presented in Waters et al. (2000). A varying propagation speed following a given velocity profile can be applied to the model Gaussian pulses, in a fashion similar to the varying-speed pulse propagation in Sarris et al. (2002), even though the single pulse in Sarris et al. (2002) was radically different in character from the propagation of compressional pulses in the ULF range, and simulated the field reconfiguration of the dipolarization process during a substorm (e.g. Reeves et al., 1996). An Alfvénic velocity profile with dampening characteristics, such as described above, would make the model able to reproduce ULF fluctuation signatures in a more realistic way also away from geosynchronous orbit.

It is still a matter of debate if and under what conditions ULF electromagnetic fluctuations can lead to sufficient transport of electrons to create the orders-of-magnitude flux increases that are often observed, in particular in regions of

lower $L$, where particle convection by induced electric fields alone cannot explain such high fluxes. A necessary condition for radial diffusion to be successful as an acceleration mechanism is a sufficient source population, the importance of which has been stressed by many authors (e.g. Baker et al., 1998b, and references therein). Such source populations can be provided, for example, by substorm-related particle injections. These processes have a convective character that can transport particles in a way that is very different from diffusion. The above physical process itself might have no connection to increased ULF power, although particle injections and increased ULF power are both usually correlated to intense magnetospheric activity and increased solar wind velocity (Mann et al., 2004). However, particle injections are not often observed deeply inside of geosynchronous orbit. Sarris et al. (2002) and Sarris and Li (2005) have shown that there is an inner limit to the distance where energetic particles can be transported during a substorm injection. Enhanced particle populations are often observed inwards of this region, and radial diffusion by ULF perturbations could be one of the mechanisms that can transport this source population into the inner magnetosphere.

## 6 Summary – Conclusions

A model of magnetospheric variability in the ULF regime has been presented: In this model the simulated electromagnetic field fluctuations represent the compressional, poloidal mode of ULF perturbations. The model is constructed by a superposition of a large number of electric and consistent magnetic pulses that are initialized at random initial radial distances with random amplitudes, in order to reproduce a realistic broadband fluctuation. The amplitude and spatial characteristics of the pulses were selected so as to produce field signatures that are often observed at geosynchronous orbit. The spectral characteristics of the model fields were compared to GOES-8 magnetic field measurements, and it was found that the model mimics closely realistic states of quiet-time, large-scale, low-$m$ ULF fluctuations.

In this model of superimposed analytic pulse fields, the power of compressional oscillations can be distributed azimuthally with analytical expressions of their azimuthal modulation, simulating pulsations of different localizations. Thus the model allows us to study the diffusive effects of different modes of fluctuation. In the present study particle motion was simulated under the effect of: a) single-mode compressional fluctuations of an azimuthal modulation that corresponds to mode number $m$=1 and b) multiple-mode compressional fluctuations with mode numbers from $m$=1 to $m$=8. The diffusion coefficient of magnetic symmetric diffusion $D_{LL}^{B,Sym}$ for the two cases was determined around geosynchronous orbit from the radial transport of electrons traced in the simulation. The numerically calculated diffusion coefficients were subsequently compared to the diffusion coefficients derived theoretically by Falthammar (1965) and generalized by Fei et al. (2006). The comparison has shown that the effect of small-amplitude ULF compressional fluctuations can be described as a diffusive process and approximated by the radial diffusion coefficients. The numerical calculations of the diffusion coefficient were found to be lower than the theoretical estimates by approximately a factor of two, consistently for both simulations; a speculation for this factor of $\sim$2 discrepancy involves correctly counting only geoeffective waves when calculating the Power Spectral Density to be used in the theoretical formulations of the diffusion coefficient.

By comparing the effects of the various modes in the multiple-mode simulation it was found that most contribution to the radial diffusion of electrons of a single $\mu$-value comes from the lowest mode number; hence, the diffusion coefficient, $D_{LL}^{B,Sym}$, as derived by Falthammar (1965) for non-relativistic particles, is sufficient to describe the effects of low-mode fluctuations, such as the ones in the simulations performed. The generalized derivation by Fei et al. (2006) for relativistic particles is more capable of correctly describing the diffusion coefficient in the case of higher-mode fluctuations.

*Acknowledgements.* T. E. Sarris wishes to thank S. Elkington, A. Chan, J. Albert and B. Lysak for very insightful comments and fruitful conversations.

Topical Editor I. A. Daglis thank two referees for their help in evaluating this paper.

## References

Albert, J. M., Brautigam, D. H., Hilmer, R. V., and Ginet, G. P.: Dynamic Radiation Belt Modeling at Air Force Research Laboratory, Space Weather, Geophysical Monograph 125, edited by: Song, P., Singer, H. J., and Siscoe, G. L., 281–287, 2001.

Alfvén, H. and Falthammar, C. G.: Cosmical Electrodynamics, Oxford Univ. Press, New York, 1963.

Anderson, B. J., Engebretson, M. J., Prounds, S. P., Zanetti, L. J., and Potemra, T. A.: A statistical study of Pc3-5 pulsations observed by the AMPTE/CCE magnetic ®eld experiment 1. Occurrence distribution, J. Geophys. Res., 95, 10 495–10 523, 1990.

Arthur, C. W., McPherron, R. L., and Hughes, W. J.: A statistical study of Pc3 magnetic pulsations at synchronous orbit, ATS 6., J. Geophys. Res., 82, 1149, 1977.

Baker, D. N., Blake, J. B., Klebesadel, R. W., and Higbie, P.R.: Highly relativistic electrons in the Earth's outer magnetosphere, 1., lifetimes and temporal history 1979–1984, J. Geophys. Res., 91, 4265–4276, 1986.

Baker, D. N., Kanekal, S., Blake, J. B., Klecker, B., and Rostoker, G.: Satellite anomalies linked to electron increase in the magnetosphere, Eos Trans., AGU, 75, 401, 1994.

Baker, D. N., Li, X., Turner, N., et al.: Recurrent geomagnetic storms and relativistic electron enhancements in the outer magnetosphere: ISTP coordinate measurements, J. Geophys. Res., 102, 14 141–14 148, 1997.

Baker, D. N., Allen, J., Kanekal, S. G., and Reeves, G. D.: Disturbed space environment may have been related to pager satellite failure, Eos Trans., AGU, 79, 477, 1998a.

Baker, D. N., Pulkkinen, T. I., Li, X., Kanekal, S. G., Blake, J. B., Selesnick, R. S., Henderson, M. G., Reeves, G. D., Spence, H. D., and Rostoker, G.: Coronal mass ejections, magnetic clouds, and relativistic magnetospheric electron events: ISTP, J. Geophys. Res., 103, 17 279–17 292, 1998b.

Barnes, A.: Hydromagnetic waves, turbulence, and collisionless processes in the interplanetary medium, in: Solar-Terrestrial Physics: Principles and Theoretical Foundations, edited by: Carovillano, R. L. and Forbes, J. M., pp.155–199, D. Reidel Publishing Company, Dordrecht, 1983.

Bourdarie, S., Boscher, D., Beutier, T., Sauvaud, J. A., and Blanc, M.: Electron and proton radiation belt dynamics simulations during storm periods, a new asymmetric convective-diffusive model, J. Geophys. Res., 102, 17 541, 1997.

Brautigam, D. H. and Albert, J. M.: Radial diffusion analysis of outer radiation belt electrons during the 9 October 1990, magnetic storm, J. Geophys. Res., 105, 291–309, 2000.

Brizard, A. J., and Chan, A. A.: Relativistic bounce-averaged quasilinear diffusion equation for low-frequency electromagnetic fluctuations, Phys. of Plasmas, Vol. 8, 11, doi:10.1063/1.1408623, 2001.

Burlaga, L. F. and Ogilvie, K. W.: Causes of sudden commencements and impulses, J. Geophys. Res., 74, 2815, 1969.

Chen, L. and Hasegawa, A.: A theory of long-period magnetic pulsations, 1, Steady state excitation of field line resonance, J. Geophys. Res., 79, 1024, 1974.

Dungey, J. M.: Hydromagnetic waves, in Geophysics, the Earth's Environment, edited by DeWitt, C., Hieblot, J. and Leleau, A., Gordon and Breach, Newark, N. J., 1963.

Dungey, J. M.: Effects of electromagnetic perturbations on particles trapped in the radiation belts, Space Sci. Rev., 4, 199–222, 1964.

Elkington, S. R., Hudson, M. K., and Chan, A. A.: Acceleration of relativistic electrons via drift–resonant interaction with toroidal-mode Pc5 ULF oscillations, Geophys. Res. Lett. 26, 3273, 1999.

Elkington, S. R., Hudson, M. K., and Chan, A. A.: Resonant acceleration and diffusion of outer zone electrons in an asymmetric geomagnetic field, J. Geophys. Res. 108, doi:10.129/2001JA009202, 2003.

Falthammar, C. G.: Effects of time-dependent electric and magnetic fields on geomagnetically trapped radiation, J. Geophys. Res., 70, 2503, 1965.

Falthammar, C. G.: Radial diffusion by violation of the third adiabatic invariant, in Earth's Particles and Fields, Reinhold, New York, p. 157, 1968.

Fei, Y., Chan, A. A., Elkington, S. R., and Wiltberger, M. J.: Radial diffusion and MHD-particle simulations of relativistic electron transport by ULF waves in the September 1998 storm, in print, J. Geophys. Res., 2006.

Francis, W. E., Green, M. J., and Dessler, A. J.: Hydromagnetic propagation of sudden commencements of magnetic storms, J. Geophys. Res., 64, 1643, 1959.

Friedel, R. H. W., Reeves, G. D., and Obara, T.: Relativistic electron dynamics in the inner magnetosphere-a review, J. Atmos. Solar Terr. Phys., 64, 265, 2002.

Green, J. C., and Kivelson, M. G.: Relativistic electrons in the outer radiation belt: Differentiating between acceleration mechanisms, J. Geophys. Res., 109, doi:10.1029/2003JA010153, 2004.

Greenstadt, E. W., Singer, H. J., Russell, C. T., and Olson, J. V.: IMF orientation, solar wind velocity, and Pc 3-4 signals: a joint distribution, J. Geophys. Res. , 84(A2), 527-32, 1979.

Greenstadt, E. W., Russell, C. T., and Hoppe, M.: Magnetic field orientation and superthermal ion streams in the earth's foreshock, J. Geophys. Res. , 85(A7), 3473–3479, 1980.

Gussenhoven, M. S., Mullen, E. G., Brautigam, D. H., Holeman, E., and Jordan, C.: Preliminary comparison of dose measurements on CRRES to NASA model predictions, IEEE Trans. Nucl. Sci., 38, 1655, 1991.

Hasegawa, A., Tsui, K. H., and Assis, A. S.: A theory of long-period mag-netic pulsations, 3, Local field line oscillations, Geophys. Res. Lett., 10 765, 1983.

Hedgecock, P. C.: Giant Pc 5 pulsations in the outer magnetosphere: A survey of HEOS-1 data, Planet. Space Sci., 24, 921–935, 1976.

Hudson, M. K., Kotelnikov, A. D., Li, X., et al.: Simulation of Proton Radiation Belt Formation During the 24 March 1991 SSC, Geophys. Res. Lett., 22, 291, 1995.

Jacobs, J. A., Kato, Y., Matsushita, S., and Troitskaya, V. A.: Classification of geomagnetic micropulsations, J. Geophys. Res., 69, 180, 1964.

Kepko, L., Spence, H. E., and Singer, H.: ULF waves in the solar wind as direct drivers of magnetospheric pulsations, Geophys. Res. Lett., 29, doi:10.1029/2001GL014405, 2002.

Kivelson, M. G. and Southwood, D. J.: Resonant ULF waves: a new interpretation, Geoph. Res. Lett., 12, 49–52, 1985.

Kivelson, M. G. and Russel, C. T.: Introduction to Space Physics, Cambridge University Press, 1995.

Lanzerotti, L. J., Maclennan, C. G., and Schulz, M.: Radial diffusion of outer-zone electrons: An empirical approach to the third-invariant violation, J. Geophys. Res., 75, 5351–5371, 1970.

Lanzerotti, L. J. and Morgan, C. G.: ULF geomagnetic power near L=4, 2, Temporal variation of the radial diffusion coefficient for relativistic electrons, J. Geophys. Res., 78, 4600, 1973.

Lanzerotti, L. J., Webb, D. C., and Arthur, C. W.: Geomagnetic field fluctuations at synchronous orbit 2. Radial diffusion, J. Geophys. Res., 83, 3866, 1978.

Lee, D. H. and Lysak, R. L.: MHD waves in a three-dimensional dipolar magnetic field: A search for Pi2 pulsations, J. Geophys. Res., 104, 28 691–28 699, 1999.

Li, X., Roth, I., Temerin, M., Wygant, J., Hudson, M. K., and Blake, J. B.: Simulation of the prompt energization and transport of radiation particles during the 24 March 1991 SSC, Geophys. Res. Lett., 20, 2423, 1993.

Li, X. and Temerin, M.: The electron radiation belt, Space Sci. Rev., 95, 569, 2001.

Li, X., Temerin, M., Baker, D. N., Reeves., G. D., and Larson, D.: Quantitative prediction of radiation belt electrons at geostationary orbit based on solar wind measurements, Geophys. Res. Lett., 28, 1887, 2001.

Li, X.: Variations of 0.7–6.0 MeV electrons at geosynchronous orbit as a function of solar wind, Space Weather, Vol. 2, No. 3, *S*0300610.1029/2003SW000017, 2004.

Mann, I. R. and Wright, A. N.: Finite lifetimes of ideal poloidal Alfvén waves, J. Geophys. Res., 100, 23 677–23 686, 1995.

Mann, I. R., O'Brien, T. P., and Milling, D. K.: Correlations between ULF wave power, solar wind speed, and relativistic electron flux in the magnetosphere: solar cycle dependence, J. Atmo-

sph. and Sol.-Ter. Phys., 66, 187–198, 2004.

Mathie, R. A. and Mann, I. R.: On the solar wind control of Pc5ULF pulsation power at mid-latitudes: Implications for MeV electron acceleration in the outer radiation belt, J. Geophys. Res.,106, 29 783, 2001.

Matsuoka, H., Takahashi, K., Yumoto, K., Anderson, B. J., and Sibeck, D. G.: Observation and modeling of compressional Pi3 magnetic pulsations, J. Geophys. Res., 100, 12 103, 1995.

Mozer, F. S.: Power spectra of the magnetospheric electric field, J. Geophys. Res. 76, 3651, 1971.

Nishida, A.: Ionospheric screening effects and sudden commencements, J. Geophys. Res., 69, 1761, 1964.

Northrop, T. G.: The Adiabatic Motion of Charged Particles, 29 pp., Wiley-Interscience, New York, 1963.

Obara, T., Nagatsuma, T., and Onsager, T. G.: Effects of the interplanetary magnetic field (IMF) on the rapid enhancement of relativistic electrons in the outer radiation belt during the storm recovery phase, in Fourth International Conference on Substorms, p. 215, Kluwer Acad, Norwell, Mass., 1998.

O'Brien, T. P., McPherron, R. L., Somette, D., Reeves, G. D., Friedel, R., and Singer, H.: Which magnetic storms produce relativistic electrons at geosynchronous orbit?, J. Geophys. Res., 106, 15 533, 2001.

Paulikas, G. A. and Blake, J. B.: Effects of the solar wind on magnetospheric dynamics: Energetic electrons at the synchronous orbit, in Quantitative Modeling of Magnetospheric Processes, Geophys. Monogr. Ser., 21, edited by: Olson, W. P., p. 180, AGU, Washington, D. C., 1979.

Perry, K. L., Hudson, M. K., and Elkington, S. R.: Incorporating spectral characteristics of Pc5 waves into three dimensional radiation belt modeling and the diffusion of relativistic electrons, J. Geophys. Res., 110, doi:10.1029/2004JA010760, 2005.

Radoski, H. R.: Hydromagnetic waves: Temporal development of coupled modes, Environ. Res. Pap. 559, Air Force Geophys. Lab., Hanscom AFB, 1976.

Reeves, G. D., Henderson, M. G., McLachlan, P. S., and Belian, R. D.: Radial propagation of substorm injections, in Substorms-3, edited by ESA, p. 579, ESA Publications Division, 1996.

Riley, P. and Wolf, R. A.: Comparison of diffusion and particle drift description of radial transport in the Earth's inner magnetosphere, J. Geophys. Res., 97, 16 865, 1992.

Rioul, O. and Vetterli, M.: Wavelets and Signal Processing, IEEE Signal Processing Magazine, 8, pp. 14–38, 1991.

Sarris, T. E., Li, X., Tsaggas, N., and Paschalidis, N.: Modeling energetic particle injections in dynamic pulse fields with varying propagation speeds, J. Geophys. Res., 107, 1033, doi:10.1029/2001JA900166, 2002.

Sarris, T. E. and Li, X.: Evolution of the dispersionless injection boundary associated with substorms, Ann. Geophys., 23, 877–884, 2005, http://www.ann-geophys.net/23/877/2005/.

Schulz, M. and Lanzerotti, L. J.: Particle diffusion in the radiation belts, Springer, New York, 1974.

Southwood, D. J.: Some features of field line resonances in the magnetosphere, Planet. Space Sci., 22, 492, 1974.

Stellmacher, M., Glassmeier, K. H., Lysak, R. L., and Kivelson, M. G.: Field line resonances in discretized magnetospheric models: an artifact study, Ann Geoph., 15, 614–624, 1997.

Takahashi, K., McPherron, R. L., and Greenstadt, E. W.: Factors controlling the occurrence of Pc 3 magnetic pulsations at synchronous orbit, J. Geophys. Res., 86, 5472-84, 1981.

Takahashi, K. and McPherron, R. L.: Harmonic structure of Pc 3-4 pulsations, J. Geophys. Res., 87, 1504, 1982.

Ukhorskiy, A. Y., Takahashi, K., Anderson, B. J., and Korth, H.: Impact of toroidal ULF waves on the outer radiation belt electrons, J. Geophys. Res., 110, A10202, doi:10.1029/2005JA011017, 2005.

Ukhorskiy, A. Y., Anderson, B. J., Takahashi, K., and Tsyganenko, N. A.: Impact of ULF oscillations in solar wind dynamic pressure on the outer radiation belt electrons, Geophys. Res. Lett., 33, L06111, doi:10.1029/2005GL024380, 2006.

Walker, A. D. M.: Magnetohydrodynamic Waves In Geospace: The Theory of ULF Waves and their Interaction with Energetic Particles in the Solar-Terrestrial Environment, pp. 233–244, Institute of Physics Publishing, Bristol and Philadelphia, 2005.

Waters, C. L., Samson, J. C., and Donovan, E. F.: Variation of plasmatrough density derived from magnetospheric field line resonances, J. Geophys. Res., 101, 24 737, 1996.

Waters, C. L., Harrold, B. G., Menk, F. W., Samson, J. C., and Fraser, B. J.: Field line resonances and waveguide modes at low latitudes. 2. A model, J. Geophys. Res., 105, 7763–7774, 2000.

Wright, A. N.: Dispersion and wave coupling in inhomogeneous MHD waveguides, J. Geophys. Res., 99, 159, 1994.

Wright, A. N. and Rickard, G. J.: A numerical study of resonant absorption in a magnetohydrodynamic cavity driven by broadband spectrum, Astrophys. J., 444, 458–470, 1995.

Yumoto, K.: External and internal sources of low-frequency MHD waves in the magnetopause – a review, J. Geomagn. Geoelectr., 40, 293, 1988.